# Bistable Morphing Composites with Selectively-Prestressed Laminae

Venkata Siva C. Chillara and Marcelo J. Dapino *

Smart Vehicle Concepts Center, Department of Mechanical and Aerospace Engineering
The Ohio State University, Columbus, OH 43210

## ABSTRACT

Bistable laminated composites are candidates for morphing structures as they are capable of large deflections without actuation and can exhibit drastic shape change when actuated. The coupled stable shapes of traditional thermally-cured fiber-reinforced polymeric laminates are the result of a globally-prestressed matrix and hence cannot be tailored independently. In this paper, we address this limitation by presenting an equivalent laminated composite in which mechanical prestress is applied to the matrix of selected laminae to achieve bistability; shapes are tailored individually by changing the magnitude of prestress in each lamina. The application of mechanical prestress is associated with an irreversible non-zero stress state which when combined with smart materials with controllable stress-states results in multifunctional morphing composites. The proposed bistable composite consists of a core that is sandwiched between two prestressed fiber-reinforced elastomers and is actuated by shape memory alloy wires. Composite mechanics is modeled analytically by incorporating the material and geometric nonlinearities of prestressed elastomers and the 1-D constitutive behavior of a shape memory alloy (SMA). The experimentally-validated model of the passive composite has an accuracy of 94%. A sensitivity study is conducted that shows the effects of prestress and SMA properties on composite curvature and serves as a guide for the design of active bistable composites. Simulations with the chosen parameter set resulted in the exact compensation of the nonlinear effects of applied stress and phase transformation kinetics to yield a linear response of composite curvature to Martensitic volume fraction.

**Keywords:** Bistable, morphing, shape memory, residual stress, fiber-reinforced elastomer

## 1. INTRODUCTION

Bistable composites offer opportunities for morphing structures due to their capability of drastic shape change at low energy cost. These composites require actuation only to switch from one stable deformed shape to another. Given the potential for lightweighting and design simplicity, bistable laminates are suitable for a broad range of applications: in automobiles, bistable composites could serve as adaptive body panels that switch shape at high speed to enhance aerodynamic performance;[1] in wind turbine blades, bistable elements are used as passive mechanisms for load alleviation;[2,3] a seamless multistable morphing wing contributes to improved fuel efficiency of aircraft through lightweighting.[4,5]

Imparting residual stress is an attractive approach to create curvature in a laminated composite since it is an intrinsic feature and requires no external loads. The most widely studied designs for bistability involve thermally-cured fiber-reinforced polymeric laminates (FRP) that contain residual stress at room temperature. The residual stress is caused by a mismatch in the thermal contraction of the matrix and the fiber. In FRP laminates with asymmetric fiber orientations, the potential energy associated with residual stress can have two minima corresponding to two stable shapes that are curved in opposite directions.[6] In such composites, Hyer[7] and Schlecht et al.[8] showed that the magnitude of curvature is primarily influenced by curing temperature and its direction is governed by fiber orientation.

*Further author information: (Send correspondence to M.J.D.)
M.J.D.: E-mail: dapino.1@osu.edu
V.S.C.: E-mail: chillara.1@osu.edu

Behavior and Mechanics of Multifunctional Materials and Composites 2017, edited by Nakhiah C. Goulbourne,
Proc. of SPIE Vol. 10165, 101650Y · © 2017 SPIE · CCC code: 0277-786X/17/$18 · doi: 10.1117/12.2259787

The key contributions related to design improvements in bistable FRP laminates include: augmentation of curvature using a sandwiched metal core;[9] creating bistability in symmetric FRP laminates by applying mechanical prestress to the fibers[10] and by using a hybrid layup with two metallic layers.[11] In designs based on thermally-induced bistability, residual stress spans the composite due to the presence of a continuous matrix. Global prestress yields fully-coupled equilibrium shapes, leaving little scope to tailor individual shapes. Chillara et al.[12] demonstrated a curved laminated composite with residual stress confined to the matrix of a single lamina. Based on this approach, they presented a novel bistable composite in a 0°/core/90° configuration whose stable shapes are analogous to that of a traditional FRP laminate and can be independently tailored by varying prestress in select laminae.[13]

Actuation of bistable composite plates can be achieved by recovering the in-plane strain corresponding to one stable deformed shape up to a point where the composite snaps into its second stable deformed shape. This function is typically realized either by applying an out-of-plane moment at the ends of the composite or by contraction of an planar active element. Thermal loading[14] is a simple means to achieve snap-through but may not be applicable to all operating conditions. Laminae with embedded fluid channels can be pressurized to flatten the composite[15] and subsequently snap it into its second shape. Smart materials such as piezoelectrics and shape memory alloys, capable of controllable stress-states, are lightweight actuators that can either be embedded, mounted externally, or included as a lamina in bistable composites. Schultz et al.[16] demonstrated actuation using electrically-activated piezoceramic (macro-fiber composites) laminae that are curved to conform to one of the stable shapes. While piezoelectric actuators enable a rapid snap-through, they are ineffective for snap-back due to their low strain capability (0.1 %). Kim et al.[17] combined low strain piezoelectric laminae and high strain shape memory alloy wire (6 %) to achieve rapid snap-through and relatively slow snap-back respectively.

For morphing applications where the operating frequency is a few Hz, shape memory alloys (SMA) are applicable. SMAs can be used for snap-through and snap-back due to their high strain capability. Dano and Hyer[18] presented an analytical model for the actuation of bistable FRP laminates using SMAs. They modeled SMA wire in a tendon (straight) configuration and validated the simulated shape transition using experiments. However, SMA actuation is more feasible for practical applications when used in a laminar configuration. Simoneau et al.[19] and Lacasse et al.[20] developed an FE model for laminated composites that are actuated using embedded SMAs; the relationship between the composite's material and geometric properties, and actuation effort was studied for a monostable composite with one-way actuation. Prototypes of SMA-actuated bistable composites were designed and fabricated by Hufenbach et al.;[21,22] SMAs wires were installed so as to follow the curvature of the composite. Although designs of SMA-actuated laminated composites exist, two-way actuation, where activation of one SMA results in a shape transition that induces a phase-transformation in the antagonistic SMA, is yet to be fully understood.

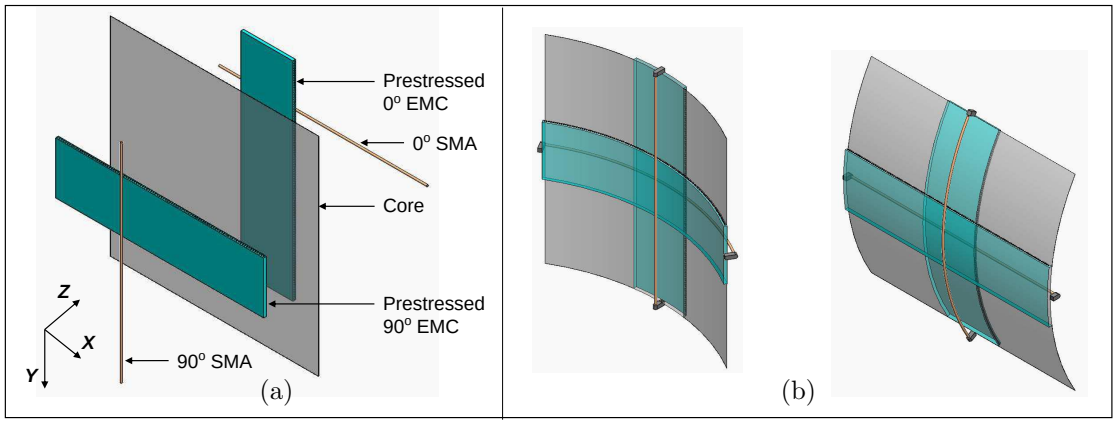


Figure 1. (a) Configuration and (b) stable shapes of an SMA-actuated mechanically-prestressed bistable composite.

This paper presents an asymmetric bistable composite that consists of a stress-free isotropic core sandwiched between two mechanically-prestressed fiber-reinforced elastomers (Figure 1). Fiber-reinforced elastomers, also

known as elastomeric matrix composites (EMC), are applied in the form of strips with fibers aligned in the width direction (90° orientation) to achieve near-zero in-plane Poisson's ratio.[23,24] Two such 90° EMC strips are oriented in the composite such that the respective fibers in each strip are at 90° and 0° with respect to the $X$ axis (Figure 1). Mechanical prestrain is applied to both EMCs in the matrix-dominated direction prior to lamination. The resulting composite is bistable with cylindrical curvatures that are orthogonal to each other. A special feature in composites with orthogonal EMCs is that the resulting cylindrical shapes are weakly coupled. The magnitude of each curvature is independent of prestress in the EMC on the convex face and can be tailored by varying the prestress in the EMC on the concave face. The modulus and thickness of the core, and the width of each EMC influence both curvatures. EMC width is limited to a fraction of core width to avoid restriction in curvature due to the high-modulus fibers.

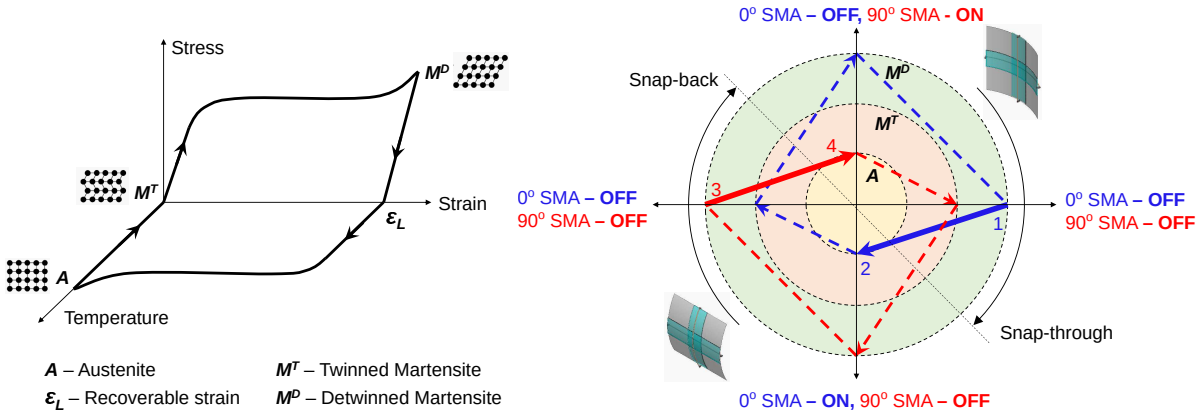


(a) (b)

Figure 2. (a) Stress-strain behavior of a shape memory alloy, (b) operating modes of SMAs in a bistable laminate.

The proposed composite is actuated using SMA wires that are assembled in the 90° and 0° orientations as shown in Figure 1. The high plastic strain in an SMA that is used for actuation is a result of a transformation between the high-temperature Austenite and low-temperature Martensite phases. Below Martensite temperature, the SMA transforms from twinned to detwinned Martensite when stress is applied (Figure 2(a)). Heating the detwinned SMA beyond the Austenite start temperature converts the SMA to Austenite. Upon cooling, the Austenitic SMA returns to the twinned Martensite phase. In a composite that is initially curved about the $Y$ axis, the 0° and 90° Martensitic SMAs are installed in the detwinned and twinned states respectively. Heating the detwinned 0° SMA to Austenite leads to a decrease in curvature about the $Y$ axis followed by snap-through to the curvature about $X$ axis. Post snap-through, the 90° SMA undergoes detwinning as the composite attains equilibrium. For snap-back, the 90° SMA is heated to its Austenitic phase and the 0° SMA gets detwinned as a consequence of shape transition. The phase diagram for both SMAs, associated with the morphing of the bistable composite, is shown in Figure 2(b). The novelty in this paper is a fully-coupled analytical model that describes the interaction between smart-material actuators and prestressed laminae in morphing composites.

## 2. COMPOSITE FABRICATION AND EXPERIMENTS FOR MODEL VALIDATION

The analytical model for a passive mechanically-prestressed bistable composite has been validated experimentallly by Chillara et al.[13] Multiple composite samples were fabricated and their shapes were measured using a 3D motion capture technique. Each of the 90° and 0° EMCs in the composite is stretched between a pair of grips and held at a given prestrain for lamination with a spring steel core (Figure 3 (a)). The laminae are bonded using a flexible, room temperature vulcanized silicone adhesive that cures in 24 hours. Pressure is applied to the bonded region using clamps to ensure a uniform bond. The ends of the prestressed EMCs are wrapped around and bonded to the core to prevent delamination over time; the wrap-around of the EMC had no visible effect on composite curvature. The finished composite samples, shown in Figure 3(b), exhibit two stable shapes with orthogonal curvatures. The EMCs are prepared by saturating unidirectional carbon fibers with uncured silicone

rubber and then sandwiching them between a pair of pre-cured silicone rubber skins. The box dimensions of the fabricated samples are 152.4 × 152.4 × 4.2 (mm).

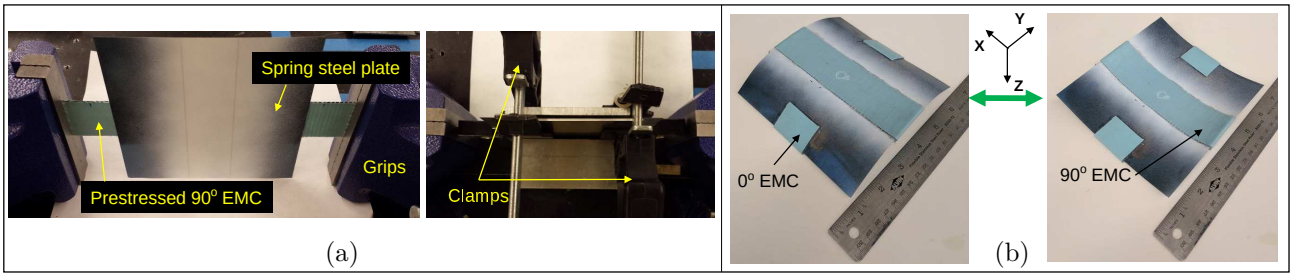


Figure 3. (a) Fabrication process and (b) stable shapes of a mechanically-prestressed bistable composite.

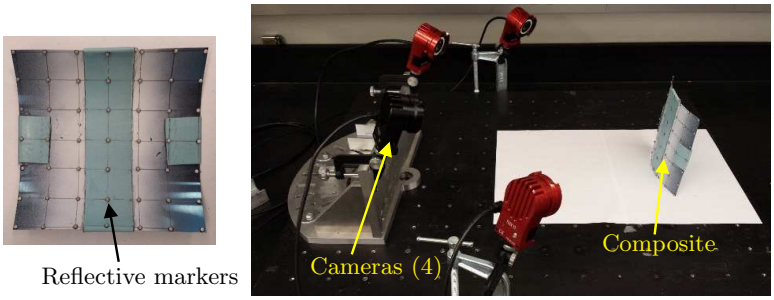


Figure 4. Measurement of composite shapes using a 3D motion capture system.

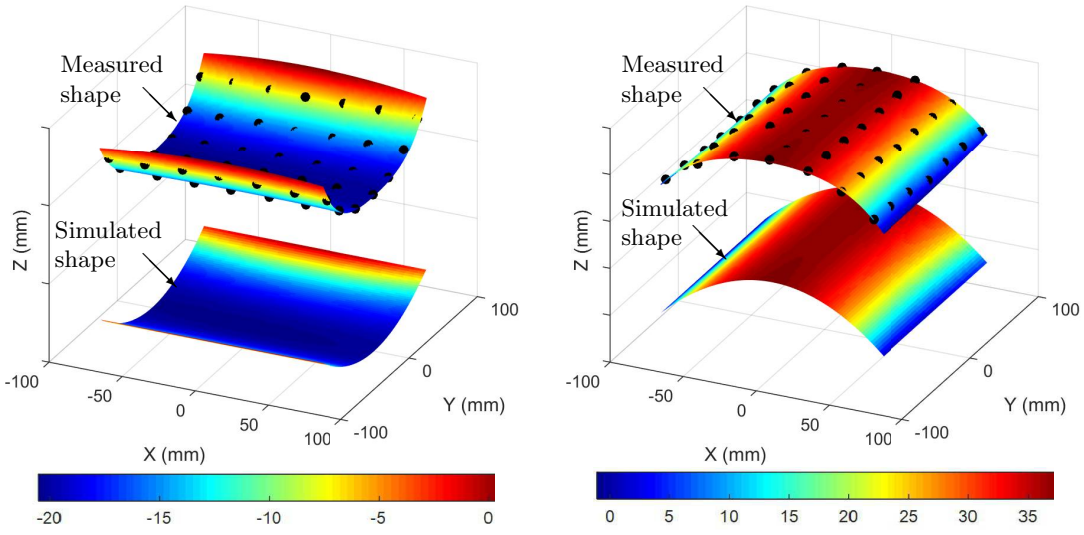


Figure 5. Measured and calculated composite shape in three dimensions. (a) Curvature relative to the $X$ axis and (b) curvature relative to the $Y$ axis.

The motion capture technique involves the tracking of reflective markers attached to the composite using a set of cameras (Figure 4). The composite had forty nine hemispherical markers of 3 mm diameter placed in a 7 × 7 grid. The coordinates of these markers were mapped using an OptiTrack (Natural Point Inc.) motion

capture system. The four cameras used in the experiment have a resolution of 1.3 megapixels and were calibrated to an accuracy of 0.03 mm within a capture volume of 305 ° 305 ° 305 (mm). The cameras are placed such that each marker is always visible to three cameras at least. The recorded marker coordinates were fit using a quartic-quadratic polynomial to obtain the shape of the composite. The measured shapes, shown in Figure 5, were found to be in agreement with the simulated shapes. The analytical model was tested using composite samples with various EMC prestrains and was found to have a maximum error of 6% in the calculation of the equilibrium shapes of the composite. Based on this validated model, the model for the actuation of a bistable composite using shape memory alloys is presented in the following section.

## 3. ANALYTICAL MODEL

### 3.1 Model of a bistable composite

The proposed bistable composite is modeled as a laminated plate in accordance with classical laminate theory.[25] For thermally-cured bistable FRP laminates, the room-temperature shapes were modeled analytically by calculating the in-plane strains and out-of-plane deflection through strain energy minimization.[7,26,27] Strains were described using nonlinear expressions as per Lagrangian formulation to explain the mechanics of the composite. A similar analytical approach is employed in this paper to describe the shapes of a mechanically-prestressed bistable laminate (Figure 6). In our composite, residual stress is a function of the material and geometric nonlinearities associated with the large strain of a hyperelastic material such as an EMC; for thermally-cured FRP bistable composites, stress is linearly related to curing temperature.

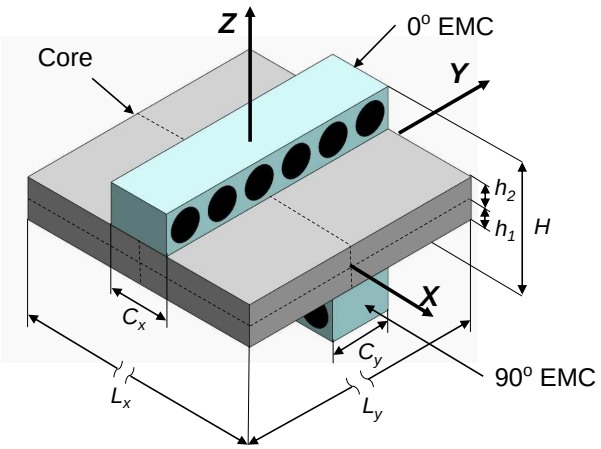


Figure 6. Schematic representation of a passive mechanically-prestressed bistable laminate.

Based on Von Karman's hypothesis, strains of the composite are written as:

$$\epsilon_x = \frac{\partial u}{\partial x} + \frac{1}{2}\left(\frac{\partial w}{\partial x}\right)^2, \tag{1}$$

$$\gamma_{xy} = \frac{\partial u}{\partial y} + \frac{\partial v}{\partial x} + \frac{\partial w}{\partial x}\frac{\partial w}{\partial y}, \tag{2}$$

$$\epsilon_y = \frac{\partial v}{\partial y} + \frac{1}{2}\left(\frac{\partial w}{\partial y}\right)^2. \tag{3}$$

The displacements $u$, $v$, and $w$ of an arbitrary point on the composite in the cartesian coordinate system ($X$, $Y$,

$Z$) are expressed in terms of the displacements $u_0$, $v_0$, and $w_0$ of the geometric mid-planes as:

$$u(x,y,z) = u_0(x) - z\frac{\partial w_0}{\partial x}, \tag{4}$$

$$v(x,y,z) = v_0(y) - z\frac{\partial w_0}{\partial y}, \tag{5}$$

$$w(x,y,z) = w_0(x,y). \tag{6}$$

Strain of an arbitrary plane $z$ of the composite is obtained by substituting (4) - (6) into (1) - (3):

$$\epsilon_x = \frac{\partial u_0}{\partial x} + \frac{1}{2}\left(\frac{\partial w_0}{\partial x}\right)^2 - z\left(\frac{\partial^2 w_0}{\partial x^2}\right), \tag{7}$$

$$\gamma_{xy} = \frac{\partial u_0}{\partial y} + \frac{\partial v_0}{\partial x} + \frac{\partial w_0}{\partial x}\frac{\partial w_0}{\partial y} - 2z\left(\frac{\partial^2 w_0}{\partial y \partial x}\right), \tag{8}$$

$$\epsilon_y = \frac{\partial v_0}{\partial y} + \frac{1}{2}\left(\frac{\partial w_0}{\partial y}\right)^2 - z\left(\frac{\partial^2 w_0}{\partial y^2}\right), \tag{9}$$

Equations (7) - (9) are written in terms of mid-plane strains ($\epsilon_x^0, \epsilon_y^0, \gamma_{xy}^0$ ) and curvatures ($\kappa_x^0, \kappa_y^0, \kappa_{xy}^0$) as:

$$\epsilon_x = \epsilon_x^0 + z\kappa_x^0, \qquad \gamma_{xy} = \gamma_{xy}^0 + z\kappa_{xy}^0, \qquad \epsilon_y = \epsilon_y^0 + z\kappa_y^0, \tag{10}$$

such that

$$\kappa_x^0 = -\frac{\partial^2 w_0}{\partial x^2}, \quad \kappa_{xy}^0 = -2\frac{\partial^2 w_0}{\partial y \partial x}, \quad \kappa_y^0 = -\frac{\partial^2 w_0}{\partial y^2}. \tag{11}$$

Strains $\epsilon_x^0$ and $\epsilon_y^0$, and displacement $w_0$ are approximated as:

$$\epsilon_x^0 = c_{00} + c_{20}x^2 + c_{11}xy + c_{02}y^2, \tag{12}$$

$$\epsilon_y^0 = d_{00} + d_{20}x^2 + d_{11}xy + d_{02}y^2, \tag{13}$$

$$w_0(x) = \frac{1}{2}(ax^2 + bxy + cy^2). \tag{14}$$

Displacements $u_0$ and $v_0$, required for the calculation of $\gamma_{xy}$, are obtained through integration of (1) and (3):

$$u_0(x,y) = c_{00}x + f_1 y + \frac{1}{2}(c_{11} - \frac{ab}{2})x^2 y + (c_{02} - \frac{b^2}{8})xy^2 + \frac{1}{3}(c_{20} - \frac{a^2}{2})x^3 + \frac{1}{3}f_3 y^3, \tag{15}$$

$$v_0(x,y) = f_1 x + d_{00}y + \frac{1}{2}(d_{11} - \frac{cb}{2})xy^2 + (d_{20} - \frac{b^2}{8})x^2 y + \frac{1}{3}(d_{02} - \frac{c^2}{2})y^3 + \frac{1}{3}f_2 x^3. \tag{16}$$

Substitution of (14), (15), and (16) in (8) yields an expression for $\gamma_{xy}$.

The potential energy of the system ($U_T$) can be expressed as a function of laminate properties, strains, and EMC prestrain as:

$$U_T = \int_V \left(U_1 + Q_{12}\epsilon_x\epsilon_y + U_2 + \frac{1}{2}Q_{16}\gamma_{xy}\epsilon_x + \frac{1}{2}Q_{26}\gamma_{xy}\epsilon_y + \frac{1}{2}Q_{66}\gamma_{xy}^2\right)\mathrm{d}V, \tag{17}$$

where $\{Q_{ij}\{i,j = 1,2,6\}\}$ are the plane stress-reduced stiffness parameters.[25] The limits of integration for the computation of strain energy are listed in Table 1. For linearly strained directions in a lamina, $U_1 = 0.5(Q_{11}\epsilon_x^2)$ and $U_2 = 0.5(Q_{22}\epsilon_y^2)$. For the prestrained directions of a 90° and a 0° EMC, the respective energy terms $U_1$ and $U_2$ are computed as the integral of $\sigma_x$ and $\sigma_y$ (nonlinear expressions) to yield functions of the form:

$$U_1^{(90)} = f(\epsilon_{90} - \epsilon_x), \qquad U_2^{(0)} = f(\epsilon_0 - \epsilon_y) \tag{18}$$

Table 1. Limits of integration for the computation of the total potential energy of a bistable laminate.

| Lamina | $x$ | $y$ | $z$ |
|---|---|---|---|
| 90° EMC | $(-L_x/2, L_x/2)$ | $(-C_y/2, C_y/2)$ | $(-H/2, -h_1)$ |
| Core | $(-L_x/2, L_x/2)$ | $(-L_y/2, L_y/2)$ | $(-h_1, h_2)$ |
| 0° EMC | $(-C_x/2, C_x/2)$ | $(-L_y/2, L_y/2)$ | $(h_2, H/2)$ |

where $\epsilon_{90}$ and $\epsilon_0$ are the prestrains in the 90° and the 0° EMCs respectively.

Prestress in the EMC is a nonlinear function of its strain due to the material's hyperelastic response. Further, measurement of the EMC's stress-strain response involves large strain that is described using a nonlinear expression;[28] stress function should be written in terms of linear strain (composite's strain). The near-zero in-plane Poisson's ratio of the EMCs allows one to use a unidirectional polynomial stress function which is computationally economical when compared to a hyperelastic stress model. For mechanically-prestressed composites, Chillara et al.[15] developed a reduced average stress function for a 90° EMC based on its measured stress-strain response. Using a similar approach, the stress function of a 90° EMC is expressed in the form of a quartic polynomial as:

$$\sigma_x = -0.698{\varepsilon_x}^4 + 2.29{\varepsilon_x}^3 - 2.306{\varepsilon_x}^2 + 1.598\varepsilon_x \quad [\text{MPa}]. \tag{19}$$

Stress $\sigma_y$ for a 0° EMC is obtained by replacing $\varepsilon_x$ in (19) with $\varepsilon_y$. The stress function of both EMCs is considered to be linear in the fiber-dominated directions. The shear response of the EMCs is also assumed to be linear and its modulus is defined as 0.8 times the linear elastic modulus in the matrix-dominated direction.[23]

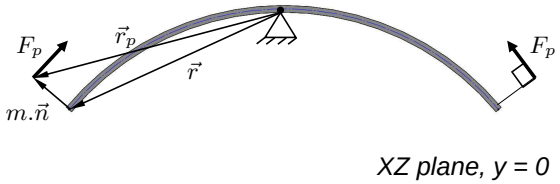


Figure 7. Actuation force applied on the composite by a shape memory alloy wire.

The actuation force generated by an SMA wire is modeled as a pair of forces ($F_p$) acting along the wire and tangential to the composite's mid-plane with an offset of $m$ in the $Z$ direction (Figure 7). Each force $F_p$ is defined in terms of the unit position vector ($\hat{r_p}$) of force application as:

$$\vec{F_p} = -F_p.\frac{\partial \hat{r_p}}{\partial x}, \tag{20}$$

where $\vec{r}_p$ is the sum of the position vector ($\vec{r}$) on the geometric mid-plane and the normal ($\hat{n}$) of magnitude $m$ at $\vec{r}$:

$$\vec{r}_p = \vec{r} + m.\hat{n}, \tag{21}$$

$$= \vec{r} + m.\frac{\left(\frac{\partial \vec{r}}{\partial x} \times \frac{\partial \vec{r}}{\partial y}\right)}{\left|\frac{\partial \vec{r}}{\partial x} \times \frac{\partial \vec{r}}{\partial y}\right|}, \qquad \text{where} \qquad \vec{r} = \Big((x+u_0)\hat{i} + (y+v_0)\hat{j} + w_0\hat{k}\Big). \tag{22}$$

The virtual work $W_p$ done by the pair of actuation forces, in a 0° SMA for example, can be written as:

$$\delta W_p = \vec{F}_p.\delta\vec{r}_p|_{\{-\frac{L_x}{2},0\}} + \vec{F}_p.\delta\vec{r}_p|_{\{\frac{L_x}{2},0\}}, \tag{23}$$

where $\vec{r}_p$ is a function of composite displacements that are described in (14) - (16). When one SMA is activated to morph the composite from one cylindrical shape to another, it is assumed that no work is done on the inactive SMA until the onset of snap-through.

The equilibrium curvatures of the composite are calculated as a function of the applied actuation force $F_p$ using a variational approach:

$$\delta(U_T - W_p) = \sum_{i=1}^{14} \frac{\partial(U_T - W_p)}{\partial c_i} = 0, \quad \text{where} \quad c_i = \{a, b, c, c_{00}, c_{20}, c_{11}, c_{02}, d_{00}, d_{20}, d_{11}, d_{02}, f_1, f_2, f_3\}. \quad (24)$$

The nonlinear algebraic equations resulting from (24) are solved for $c_i$ using the Newton-Raphson method. The resulting set of equilibrium curvatures correspond to a stable shape when the Jacobian of the system of equations is a positive definite matrix. The stable shapes of the composite are related to the thermal actuation input to the SMA by treating $F_p$ as an internal force.

### 3.2 1-D model of an SMA actuator

The pair of forces $F_p$ correspond to mechanical stress associated with the recoverable plastic strain of a shape memory alloy. This plastic strain is a result of the phase transformation between high-symmetry Austenite and low-symmetry Martensite. Tanaka et al.[29] modeled the constitutive behavior of an SMA in 1-D using thermodynamic relations; the kinetic law, describing the volume fraction of Martensite, was derived to be an exponential function. Liang and Rogers[30] modeled the phase transformation using a cosine function. Brinson[31] presented a cosine-based kinetic law that describes the Martensitic volume fraction as a sum of stress-induced and temperature-induced components. 1-D models can also be obtained by simplifying 3D constitutive models such as those presented by Boyd and Lagoudas,[32] and Ivshin and Pence.[33] Based on the fact that accuracy is not adversely affected by the choice of the model,[34] the Brinson[31] model is chosen to describe the mechanics of an SMA in the proposed bistable composite.

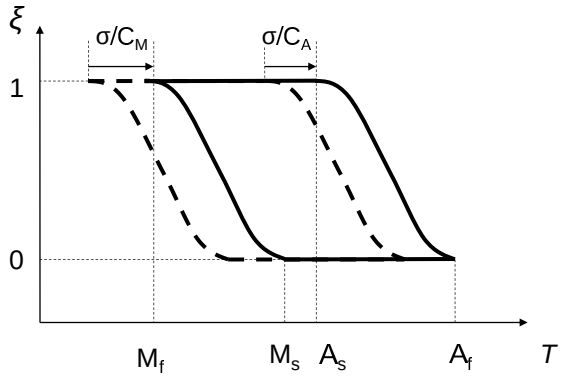


Figure 8. Phase transformation diagram of a typical 1-D shape memory alloy.

The one-dimensional constitutive law for a shape memory alloy can be written as:

$$\sigma - \sigma_0 = E(\xi)(\epsilon - \epsilon_0) + \Theta(T - T_0) + \Omega(\xi)(\xi - \xi_0) \quad (25)$$

where $\epsilon, T$, and $\xi$ are the strain, temperature, and Martensite volume fraction of the material. $E, \Theta$, and $\Omega$ are the Young's modulus, stress-temperature coefficient, and phase transformation coefficient. $E$ and $\Omega$ are calculated in terms of $\xi$ using the rule of mixtures as:

$$E(\xi) = E_A + \xi(E_M - E_A), \qquad \Theta(\xi) = \alpha_A + \xi(\alpha_M - \alpha_A), \quad (26)$$

where $\alpha_M$ and $\alpha_A$ are the coefficients of thermal expansion in the Martensite and Austenite phases respectively. Further, $\Omega = -\epsilon_L E(\xi)$, where $\epsilon_L$ is the measured maximum recovery strain.

The kinetics of phase transformation of the SMA is influenced by stress and temperature and is described using a cosine function (Figure 8). For transformation from Martensite to Austenite, when $C_A(T - A_f) < \sigma < C_A(T - A_s)$ :

$$\xi = \frac{\xi_0}{2}\left\{ \cos\left( \frac{\pi}{A_s - A_f}(T - A_s - \frac{\sigma}{C_A}) \right) + 1 \right\}, \quad (27)$$

where $C_A$ is the stress-temperature coefficient for the Austenite phase, and $A_s$ and $A_f$ are the Austenite start and finish temperatures respectively. For transformation from Austenite to Martensite, when $T > M_s$ and $\sigma_s^{cr} + C_M(T - M_s) < \sigma < \sigma_f^{cr} + C_M(T - M_s)$:

$$\xi = \frac{1-\xi_0}{2}\cos\left\{\frac{\pi}{\sigma_s^{cr}-\sigma_f^{cr}}(\sigma - \sigma_f^{cr} - C_M(T-M_s))\right\} + \frac{1+\xi_0}{2}. \tag{28}$$

where $C_M$ is the stress-temperature coefficient for the Martensite phase, $M_s$ is Martensite start temperature, and $\sigma_s^{cr}$ and $\sigma_f^{cr}$ are the critical stresses corresponding to the start and finish of phase transformation.

### 3.3 Composite actuation using SMA wires

Two-way actuation of a 90° EMC/core/0° EMC bistable composite is achieved by activating SMAs oriented in the 90°/0° configuration (Figure 1); the said SMA orientation is chosen for minimal actuation effort. Upon actuation (contraction) of the 0° SMA, the composite snaps from curvature $\kappa_{x0}$ to $\kappa_{y0}$. The snap-through phenomenon initiates a stress-induced transformation in the 90° SMA , beyond a critical stress, from twinned to detwinned Martensite (elongation). Activating the 90° SMA results in snap-back followed by the elongation of the 0° SMA back to its initial length.

Installation of SMA wires in a laminar configuration allows their strain to be defined in terms of composite strain by substituting $z$ with $m$ in (10). The length of a 0° SMA that is installed on a curved composite in the detwinned Martensite phase, is written in terms of Austenitic length ($L_A$) and equilibrium shape ($\epsilon_{x0}^{(s)}, \kappa_{x0}^{(s)}$) as $L_A(1+\epsilon_L) = L_x(1+\epsilon_{x0}^{(s)} + m\kappa_{x0}^{(s)})$. The length ($L_i$) of the 0° SMA at an intermediate shape during actuation is given by $L_i = L_x(1+\epsilon_{x0}^{(i)} + m\kappa_{x0}^{(i)})$. The actuation strain of the 0° SMA, defined as $(L_i - L_A)/L_A$, is calculated to be:

$$\epsilon = \frac{(1+\epsilon_{x0}^{(i)} + m\kappa_{x0}^{(i)})(1+\epsilon_L)}{(1+\epsilon_{x0}^{(s)} + m\kappa_{x0}^{(s)})} - 1. \tag{29}$$

The stroke $\epsilon$, computed for $F_p$ ranging from zero (equilibrium) to snap-through load, is substituted in (25) to calculate the corresponding temperature range for the actuation of the 0° SMA. Stress $\sigma$ is computed as $F_p/(\pi D^2)$, where $D$ is the diameter of the SMA wire.

Post snap-through, the 90° SMA is under tension with reaction forces $F_p$ acting at $(0, -L_y/2)$ and $(0, L_y/2)$. The magnitude of $F_p$ is unknown and is calculated for increments of curvature by simultaneously solving the constitutive law under isothermal conditions:

$$\sigma = E(\xi)((\epsilon_y + m\kappa_y) - \epsilon_L\xi), \tag{30}$$

and the kinetic law for phase transformation given by (28). The value of $\xi$ of the 90° SMA at static equilibrium would then be used as $\xi_0$ in its actuation step (snap-back).

Table 2. Material properties and dimensions of the laminae for modeling.

| Lamina | $E_1$ (MPa) | $E_2$ (MPa) | $G_{12}$ (MPa) | $\nu_{12}$ | $\nu_{21}$ | Lg. (mm) | Wd. (mm) | Ht. (mm) |
|---|---|---|---|---|---|---|---|---|
| 90° EMC | Nonlinear | 0.4 | 1.2 | 0 | 0 | 152.4 | 38.1 | 2.032 |
| Core | 200,000 | 200,000 | 78,125 | 0.28 | 0.28 | 152.4 | 152.4 | 0.127 |
| 0° EMC | 0.4 | Nonlinear | 1.2 | 0 | 0 | 38.1 | 152.4 | 2.032 |

## 4. RESULTS AND DISCUSSION

Simulations conducted on the passive composite with material properties and dimensions of the laminae as listed in Table 2. As per the rule of mixtures, $E_2$ and $E_1$ for a 90° and 0° EMC respectively are calculated to be 40.8 GPa. This high transverse EMC modulus, comparable to the core's modulus, yields a small curvature that does not represent the actual shape of the composite. Since a constant global curvature is assumed in the model,

the transverse EMC modulus is set to 0.4 MPa such that it represents shear in the purely-elastomeric sub-layer between the core and the fiber-reinforced sub-layer in the EMC. The model for the passive bistable laminate that includes the assumption on the transverse EMC modulus was experimentally validated by Chillara et al.;[13] they also presented parametric studies on the effect of various laminae properties on the shapes of the composite.

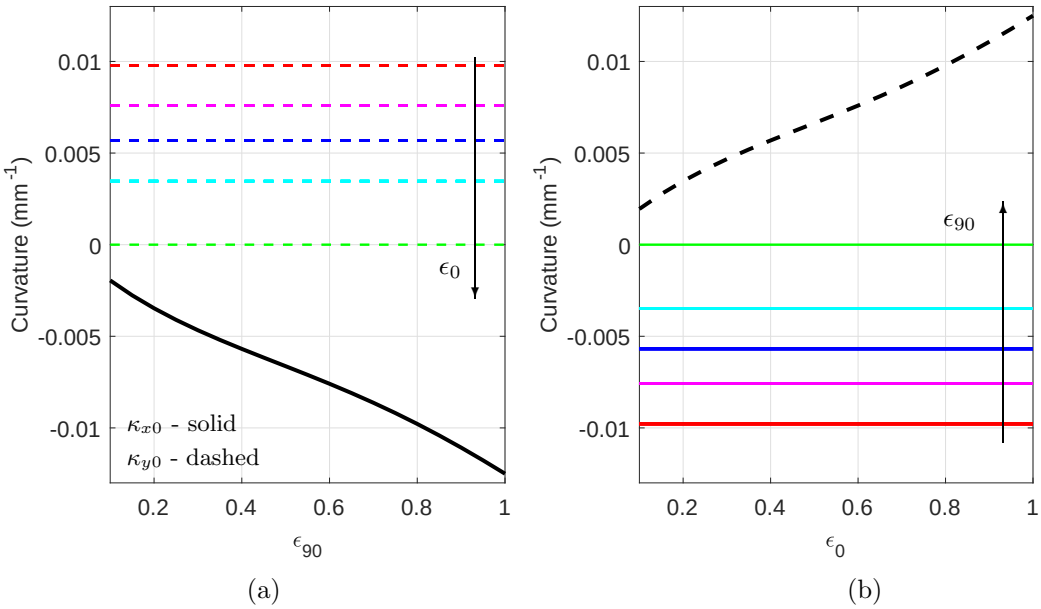


Figure 9. Cylindrical curvatures $\kappa_{x0}$ (solid) and $\kappa_{y0}$ (dashed) of a passive bistable composite as a function of prestrain in (a) the 90° EMC and (b) the 0° EMC.

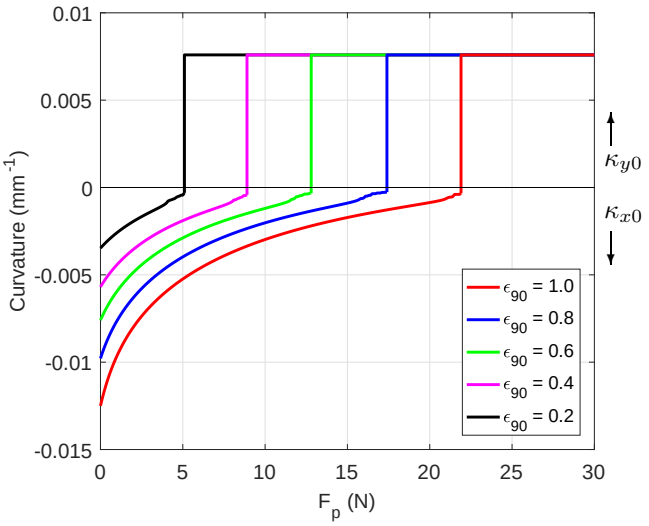


Figure 10. Actuation force generated by the SMA as a function of composite curvature.

The composite, under zero actuation input, is found to have three equilibrium shapes of which two are stable. The stable shapes are cylindrical, orthogonal, and have opposite signs. The two cylindrical shapes are defined by constant curvatures $\kappa_{x0}$ and $\kappa_{y0}$. Figures 9(a) and 9(b) respectively show the effect of prestrain in the 90°

and 0° EMCs on the set of curvatures. It is observed that each stable shape is influenced only by prestrain in the EMC on the concave face. For example, $\kappa_{x0}$ has a dependence on $\epsilon_{90}$ but not on $\epsilon_0$ (Figure 9(a)); such a response indicates a weak coupling between the stable shapes, enabling one to tailor a given curvature using only one EMC prestrain. The nonlinear dependence of $\kappa_{x0}$ on $\epsilon_{90}$ bears resemblance to the hyperelastic material response of an EMC (discussed by Chillara et al.[13]). It is worth noting that $\kappa_{x0}$ and $\kappa_{y0}$ are equal in magnitude when $\epsilon_{90}$ and $\epsilon_0$ are equal. Therefore, the range of actuation force required to achieve snap-through is unique for a given EMC prestrain (concave face).

The effect of the pair of actuation forces $F_p$ on curvature is shown in Figure 10 for various values of $\epsilon_{90}$; $\epsilon_0$ is maintained constant at 0.6. We see that the actuation force required for snap-through is higher for higher values of $\epsilon_{90}$. Further, it is apparent that the slope of $|\kappa_{x0}|$ vs. $F_p$ decreases with a decrease in $|\kappa_{x0}|$. This reduction in slope can be explained by the fact that as curvature decreases, the actuation force does more work in recovering the in-plane strain as compared to the work it does in reducing the out-of-plane deflection. In all cases of $\epsilon_{90}$, the composite snaps into the same $\kappa_y$ that corresponds to $\epsilon = 0.6$. While the assumption of constant curvature yields accurate results in the calculation of stable shapes, it is insufficient for an accurate description of actuation loads during shape transition. Higher order strain models[35,36] are more reliable for the study of actuation loads but are out of the scope of this paper.

Table 3. Measured material properties of NiTi-6 shape memory alloy wire.

| $E_M$ (GPa) | $E_A$ (GPa) | $C_M$ (MPa/° C) | $C_A$ (MPa/° C) | $\sigma_s^{cr}$ (MPa) | $\sigma_f^{cr}$ (MPa) |
|---|---|---|---|---|---|
| 20 | 40 | 6.3 | 7.5 | 10 | 120 |
| $A_s$ (° C) | $A_f$ (° C) | $M_s$ (° C) | $M_f$ (° C) | $\epsilon_L$ | |
| 48 | 62 | 23 | 7 | 0.025 | |

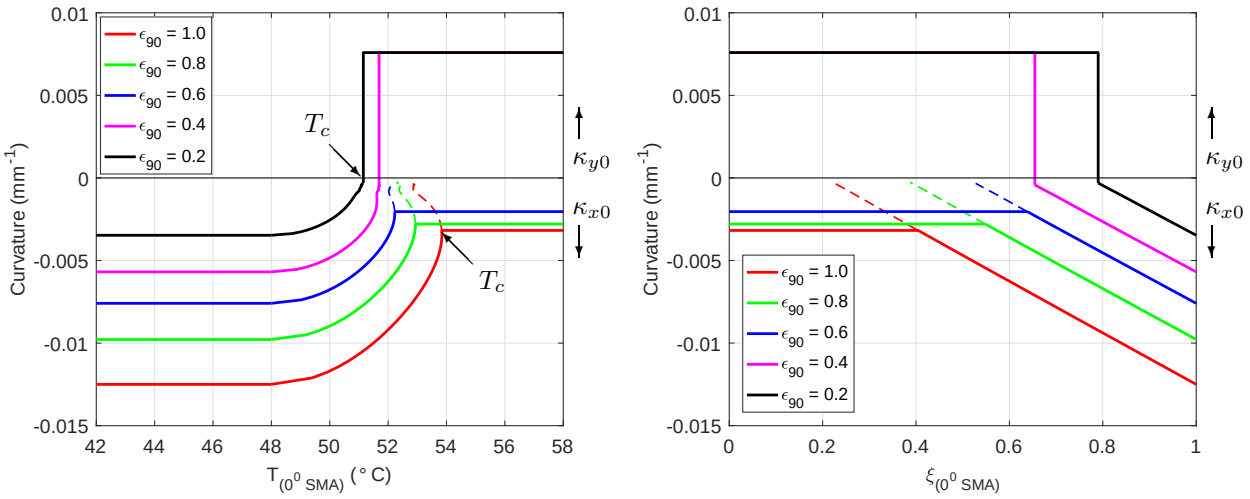


Figure 11. Effect of (a) temperature and (b) Martensitic volume fraction of a 90° SMA on composite curvature.

The actuation force $F_p$, corresponding to various values of $\kappa_{x0}$, is applied as stress on the 0° SMA. The properties of both the SMAs used for simulation correspond those of a nickel-titanium alloy called Nitinol-6 (manufactured by Fort Wayne Metals, Inc.). The material properties of Nitinol-6 were obtained by conducting isothermal tensile tests and differential scanning calorimetry on a wire of diameter 0.584 mm (Table 3). To cover a range of possible results, the diameter $D$ and maximum recoverable strain $\epsilon_L$ of the NiTi-6 SMA are chosen to be 0.889 mm and 0.08 respectively.

The quasistatic curvature of the composite is shown as a function of the temperature of the 0° SMA in Figure 11(a). The 0° SMA is assumed to be located at a distance $m = 2.54$ mm from the geometric mid-plane. The composite is initially curved about the $Y$ axis and is at room temperature ($t_0 = 25°$ C). Heating the SMA does not result in a change in $\kappa_{x0}$ until the temperature reaches the Austenite start temperature ($A_s$). Beyond $A_s$, $\kappa_{x0}$ decreases with an increase in $T$ up to a critical temperature $T_c$. For small $\epsilon_{90}$, $T_c$ represents the temperature at which snap-through occurs (e.g., black solid line in Figure 11(a)). Actuation temperature $T_c$ increases with an increase in $\epsilon_{90}$. Higher EMC prestrain results in larger curvatures, and therefore greater actuation stroke from the SMA.

For high $\epsilon_{90}$, $T_c$ is a point of inflection that indicates the minimum curvature to which the composite can be morphed; heating beyond $T_c$ has no effect on $\kappa_{x0}$ even though the recoverable strain of the SMA is sufficient for snap-through. The existence of a point of inflection $\kappa_{x0}$ can be attributed to the effect of stress on the phase transformation of the SMA (Figure 8). Stress in the SMA increases exponentially with decrease in curvature (Figure 10) and causes reversal of the SMA's transformation from Martensite to Austenite (see eq. (27)). At the point of inflection, the stress generated due to temperature change is equal to the applied stress due to reaction forces. It is mathematically possible to achieve further decrease in curvature by reducing temperature but such a solution would be non-physical (e.g., dotted red line in Figure 11(a)). Decrease in temperature brings the composite back to its initial curvature $\kappa_{x0}$ (e.g., solid red line). The variation of $\xi$ with respect to $\kappa_{x0}$ is seen to be linear (Figure 11(b)). Phase change in the SMA is higher for higher values of EMC prestrain.

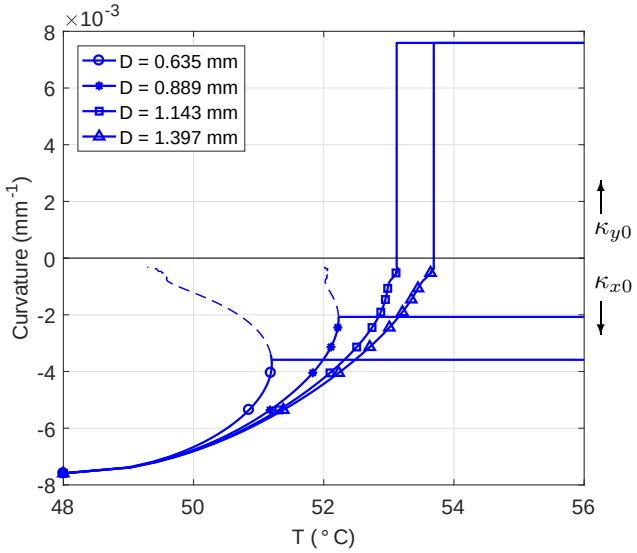


Figure 12. Effect of diameter of the 90° SMA on composite curvature.

To further examine the existence of a point of inflection $T_c$, we studied the effect of SMA wire diameter on the composite's curvature (Figure 12). For large values of $D$ such as 1.143 mm and 1.397 mm, $\kappa_{x0}$ reduces monotonically with temperature, indicating that the diameter of the wire is sufficient to achieve snap-through. Reducing wire diameter below a particular value results in an inflection in the $\kappa_{x0}$ - $T$ curve. Reduction in $D$ leads to an amplification of stress ($F_p/(\pi D^2)$) in the wire for a given value of $F_p$. By simulating curvature for a range of diameter values, one can identify the minimum cross-section of the SMA in order to operate with minimal actuation energy.

Immediately after snap-through, the 90° SMA is under tension whereas the 0° SMA is in a stress-free state when deactivated. The 90° SMA undergoes an isothermal phase transformation under the applied stress from snap-through load $F_p$ (see eq. (30)). The evolution of Martensitic volume fraction, simulated for a 90° SMA of diameter 0.584 mm, is shown as a function of $\kappa_{y0}$ in Figure 13. Phase change occurs only if the stress in the SMA immediately after snap-through lies within $\sigma_s^{cr}, \sigma_f^{cr}$; for $\epsilon_0 = 0.2$, phase transformation, shown with a dotted line, does not occur since the critical stress (22.6 MPa) is greater than the maximum stress (19.4 MPa). The initial

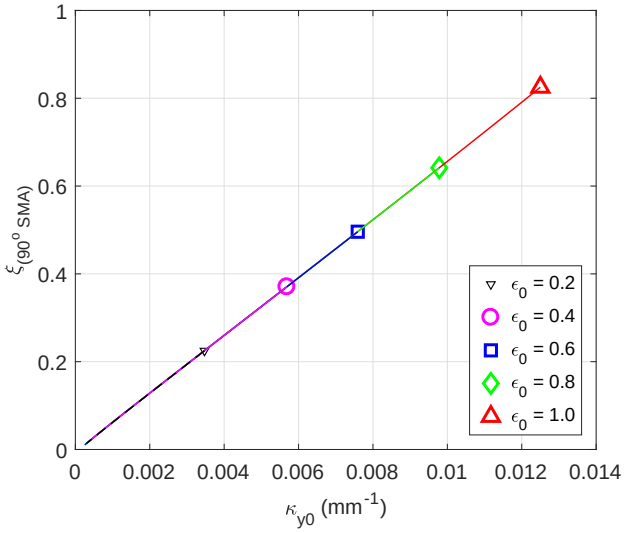


Figure 13. Post snap-through evolution of volume fraction of the 0° SMA as a function of composite curvature.

value of $\xi$ is non zero due to the difference between $T$ and $M_s$. The change in $\xi$, asssociated with plastic strain, is higher in composites with larger prestrain $\epsilon_0$. Complete transformation to Martensite ($\xi = 1$) occurs when $\epsilon_L$ is equal to the in-plane equilibrium strain of the composite at the SMA's location; in the case where $\epsilon_0 = 1$, $\xi$ is less than 1 since the in-plane strain at equilibrium (0.063) is less than $\epsilon_L$ (0.08). If $\epsilon_L$ is less than the in-plane equilibrium strain, then the composite reaches a new equilibrium shape defined by $\epsilon_L$ (not shown in Figure 13).

## 5. CONCLUDING REMARKS

A mechanically-prestressed laminated composite, in which bistability is achieved by applying prestress to select laminae, is presented as an alternative to thermally-cured FRP bistable laminates. In composites with a 90° EMC/core/0° EMC configuration, the stable shapes are weakly coupled and can be tailored independently using EMC prestrain. This weak coupling enables one to design embedded actuators that can be sequentially activated to achieve shape adaptation. An approach for the actuation of bistable composites has been illustrated using shape memory alloys as an example. The strain energy-based model of a bistable laminated composite is combined with a 1-D constitutive model of an SMA to explain the interaction between the prestressed laminae and embedded actuators. The relationships between composite curvature, EMC prestrain, and SMA parameters presented in this paper serve as a guide for actuator design.

## Acknowledgements

Financial support was provided by the member organizations of the Smart Vehicle Concepts Center, a National Science Foundation Industry/University Cooperative Research Center (www.SmartVehicleCenter.org). Additional support for S.C. was provided by a Smart Vehicle Center Graduate Fellowship. Technical advice was provided by Dr. Umesh Gandhi and Mr. Kazuhiko Mochida from Toyota Technical Center (TEMA-TTC) in Ann Arbor, MI. The experimental characterization of the NiTi-6 wire was conducted at The Ohio State University by Dr. Adam Hehr.

## REFERENCES


[1] S. Daynes and P. M. Weaver, "Review of shape-morphing automobile structures: Concepts and outlook," *Proceedings of the Institution of Mechanical Engineers, Part D: Journal of Automobile Engineering*, vol. 227, no. 11, pp. 1603–1622, 2013.

[2] X. Lachenal, S. Daynes, and P. M. Weaver, "A zero torsional stiffness twist morphing blade as a wind turbine load alleviation device," *Smart Materials and Structures*, vol. 22, no. 6, p. 065016, 2013.

[3] A. F. Arrieta, O. Bilgen, M. I. Friswell, and P. Hagedorn, "Passive load alleviation bi-stable morphing concept," *American Institute of Physics Advances*, vol. 2, no. 3, p. 032118, 2012.

[4] M. R. Schultz, "A concept for airfoil-like active bistable twisting structures," *Journal of Intelligent Material Systems and Structures*, vol. 19, no. 2, pp. 157–169, 2008.

[5] F. Mattioni, P. M. Weaver, K. D. Potter, and M. I. Friswell, "The application of thermally induced multistable composites to morphing aircraft structures," in *The 15th International Symposium on: Smart Structures and Materials & Nondestructive Evaluation and Health Monitoring*, vol. 6930, International Society for Optics and Photonics, Mar. 2008.

[6] M. W. Hyer, "Some observations on the cured shape of thin unsymmetric laminates," *Journal of Composite Materials*, vol. 15, pp. 175–194, Mar. 1981.

[7] M. W. Hyer, "The room-temperature shapes of four-layer unsymmetric cross-ply laminates," *Journal of Composite Materials*, vol. 16, no. 4, pp. 318–340, 1982.

[8] M. Schlecht and K. Schulte, "Advanced calculation of the Room-Temperature shapes of unsymmetric laminates," *Journal of Composite Materials*, vol. 33, pp. 1472–1490, Aug. 1999.

[9] S. Daynes and P. Weaver, "Analysis of unsymmetric CFRP–metal hybrid laminates for use in adaptive structures," *Composites Part A: Applied Science and Manufacturing*, vol. 41, no. 11, pp. 1712–1718, 2010.

[10] S. Daynes, K. D. Potter, and P. M. Weaver, "Bistable prestressed buckled laminates," *Composites Science and Technology*, vol. 68, pp. 3431–3437, Dec. 2008.

[11] H. Li, F. Dai, P. M. Weaver, and S. Du, "Bistable hybrid symmetric laminates," *Composite Structures*, vol. 116, pp. 782–792, Sept. 2014.

[12] V. S. C. Chillara, L. M. Headings, and M. J. Dapino, "Self-folding laminated composites for smart origami structures," in *ASME 2015 Conference on Smart Materials, Adaptive Structures and Intelligent Systems*, no. 8968, Sept. 2015.

[13] V. S. C. Chillara and M. J. Dapino, "Mechanically-prestressed bistable laminates with weakly coupled equilibrium shapes," *Composites Part B: Engineering*, vol. 111, pp. 251–260, Feb. 2017.

[14] E. Eckstein, A. Pirrera, and P. M. Weaver, "Multi-mode morphing using initially curved composite plates," *Composite Structures*, vol. 109, pp. 240–245, Mar. 2014.

[15] V. S. C. Chillara, L. M. Headings, and M. J. Dapino, "Multifunctional composites with intrinsic pressure actuation and prestress for morphing structures," *Composites Structures*, vol. 157, pp. 265–274, 2016.

[16] M. R. Schultz, M. W. Hyer, R. Brett Williams, W. Keats Wilkie, and D. J. Inman, "Snap-through of unsymmetric laminates using piezocomposite actuators," *Composites Science and Technology*, vol. 66, no. 14, pp. 2442–2448, 2006.

[17] H. A. Kim, D. N. Betts, A. I. T. Salo, and C. R. Bowen, "Shape memory Alloy-Piezoelectric active structures for reversible actuation of bistable composites," *American Institute of Aeronautics and Astronautics Journal*, vol. 48, no. 6, pp. 1265–1268, 2010.

[18] M.-L. Dano and M. W. Hyer, "SMA-induced snap-through of unsymmetric fiber-reinforced composite laminates," *International Journal of Solids and Structures*, vol. 40, pp. 5949–5972, Nov. 2003.

[19] C. Simoneau, P. Terriault, S. Lacasse, and V. Brailovski, "Adaptive composite panel with embedded SMA actuators: Modeling and validation," *Mechanics Based Design of Structures and Machines*, vol. 42, no. 2, pp. 174–192, 2014.

[20] S. Lacasse, P. Terriault, C. Simoneau, and V. Brailovski, "Design, manufacturing, and testing of an adaptive composite panel with embedded shape memory alloy actuators," *Journal of Intelligent Material Systems and Structures*, vol. 26, no. 15, pp. 2055–2072, 2014.

[21] W. Hufenbach, M. Gude, and L. Kroll, "Design of multistable composites for application in adaptive structures," *Composites Science and Technology*, vol. 62, pp. 2201–2207, Dec. 2002.

[22] W. Hufenbach, M. Gude, and A. Czulak, "Actor-initiated snap-through of unsymmetric composites with multiple deformation states," *Journal of Materials Processing Technology*, vol. 175, no. 1–3, pp. 225–230, 2006.

[23] G. Murray, F. Gandhi, and C. Bakis, "Flexible matrix composite skins for one-dimensional wing morphing," *Journal of Intelligent Materials Systems and Structures*, vol. 21, pp. 1771–1781, Nov. 2010.

[24] E. A. Bubert, B. K. S. Woods, K. Lee, C. S. Kothera, and N. M. Wereley, "Design and fabrication of a passive 1D morphing aircraft skin," *Journal of Intelligent Materials Systems and Structures*, vol. 21, pp. 1699–1717, Nov. 2010.

[25] J. N. Reddy, *Mechanics of Laminated Composite Plates - Theory and Analysis*. Boca Raton, FL: CRC Press, 1997.

[26] A. Hamamoto and M. W. Hyer, "Non-linear temperature-curvature relationships for unsymmetric graphite-epoxy laminates," *International Journal of Solids and Structures*, vol. 23, no. 7, pp. 919–935, 1987.

[27] M. L. Dano and M. W. Hyer, "Thermally-induced deformation behavior of unsymmetric laminates," *International Journal of Solids and Structures*, vol. 35, no. 17, pp. 2101–2120, 1998.

[28] L. D. Peel and D. W. Jensen, "Nonlinear modeling of fiber-reinforced elastomers and the response of a rubber muscle actuator," *Papers-American Chemical Society Division of Rubber Chemistry*, no. 30, 2000.

[29] K. Tanaka, S. Kobayashi, and Y. Sato, "Thermomechanics of transformation pseudoelasticity and shape memory effect in alloys," *International Journal of Plasticity*, vol. 2, no. 1, pp. 59–72, 1986.

[30] C. Liang and C. A. Rogers, "One-Dimensional thermomechanical constitutive relations for shape memory materials," *Journal of Intelligent Material Systems and Structures*, vol. 1, no. 2, pp. 207–234, 1990.

[31] L. C. Brinson, "One-dimensional constitutive behavior of shape memory alloys: thermomechanical derivation with non-constant material functions and redefined martensite internal variable," *Journal of Intelligent Material Systems and Structures*, vol. 4, no. 2, pp. 229–242, 1993.

[32] J. G. Boyd and D. C. Lagoudas, "A thermodynamical constitutive model for shape memory materials. part i. the monolithic shape memory alloy," *International Journal of Plasticity*, vol. 12, no. 6, pp. 805–842, 1996.

[33] Y. Ivshin and T. J. Pence, "A thermomechanical model for a one variant shape memory material," *Journal of Intelligent Material Systems and Structures*, vol. 5, no. 4, pp. 455–473, 1994.

[34] L. C. Brinson and M. S. Huang, "Simplifications and comparisons of shape memory alloy constitutive models," *Journal of Intelligent Material Systems and Structures*, vol. 7, no. 1, pp. 108–114, 1996.

[35] K. Potter, P. Weaver, A. A. Seman, and S. Shah, "Phenomena in the bifurcation of unsymmetric composite plates," *Composites Part A: Applied Science and Manufacturing*, vol. 38, no. 1, pp. 100–106, 2007.

[36] A. Pirrera, D. Avitabile, and P. M. Weaver, "Bistable plates for morphing structures: A refined analytical approach with high-order polynomials," *International Journal of Solids and Structures*, vol. 47, no. 25–26, pp. 3412–3425, 2010.